Interaction of Hydrocarbons with Clays at Reservoir Conditions: *in situ* IR and NMR Spectroscopy and X-ray Diffraction for Expandable Clays with Variably Wet Supercritical Methane: Supporting Information

Geoffrey M. Bowers[1], John S. Loring[2*], H. Todd Schaef[2], Eric D. Walter[3], Sarah D. Burton[3], David W. Hoyt[3], Sydney S. Cunniff[1], Narasimhan Loganathan[4], R. James Kirkpatrick[5]*

[1]Department of Chemistry and Biochemistry, St. Mary's College of Maryland, St. Mary's City, MD 20686

[2]Physical and Computational Sciences Directorate, Pacific Northwest National Laboratory, Richland, WA, 99352

[3]William R. Wiley Environmental and Molecular Sciences Laboratory, Pacific Northwest National Laboratory, Richland, WA, 99352

[4]Department of Chemistry, Michigan State University, East Lansing, MI, 48824

[5]Departmetns of Chemistry and Earth and Environmental Sciences, Michigan State University, East Lansing, MI, 48824

Abstract

The supporting information contains supplemental results, discussion, methods, figures, and data tables. The first section describes experimental ^{19}F MAS NMR results at 90 bar and 323 K that show no strong interactions of methane with the structural fluorine below the ditrigonal cavities in the hectorite clay. The second section reviews in greater detail prior applications of ^{129}Xe NMR and $^{13}CH_4$ NMR to probe the interaction of fluids with porous silicate materials. The third section describes our sample preparation methods in greater detail with citations. Figure S1 compares the C-H asymmetric stretching region of the IR spectra for the vacuum dried hectorite

samples, all on the same intensity scale normalized to the amount of clay. Figure S2 compares the basal XRD reflections of the four different cation-exchanged hectorites after vacuum drying and in contact with dry $scCH_4$, showing that exposure to dry $scCH_4$ does not cause expansion. Figure S3 shows the ^{19}F MAS NMR spectra associated with the supplemental results and discussion. The data tables summarize the sample masses and calculated amounts of H_2O and CH_4 in the samples for the NMR samples.

Supplementary Results and Discussion

^{19}F MAS NMR

The hectorite used in this study contains ~55% fluorine substitution on the hydroxyl sites of the octahedral sheet, and we examined the ^{19}F MAS NMR spectra before and after exposure to $scCH_4$ at 90 bar and 323 K for the Ca-hectorite to look for evidence of methane-fluorine interactions that would indicate strong CH_4 adsorption in the ditrigonal cavities, beneath which the F^- sites are located. The before and after spectra of dry Ca-hectorite are essentially identical (Figure S3), indicating that CH_4 adsorption does not cause changes in the ^{19}F NMR chemical shifts, peak widths or intensities. Thus, there does not appear to be strong electrostatic or dipolar interactions between the interlayer or external surface adsorbed CH_4 and the F^-. The spectra contain two ^{19}F resonances with spinning sideband patterns indicative of chemical shift anisotropy (Figure S3). The resonance with a center band at -182 ppm has a relatively broad spinning sideband manifold (Δ= 117 ppm) indicative of a greater chemical shift anisotropy, suggesting that the ^{19}F nuclei that contribute to it are coordinated to two Mg^{2+} and one Li^+ in the octahedral sheet. The resonance with a center band at -175 ppm has a narrower set of spinning sidebands (Δ = 86 ppm) and is more intense. We assign it to ^{19}F coordinated to three Mg^{2+} in the octahedral sheet, because this coordination causes a more symmetric bonding environment for

^{19}F. This resonance also has a larger relative intensity, which is expected assuming equal preference of F^- for F-3Mg and F-2Mg,1Li given the relative abundance of Mg^{2+} and Li^+ in the octahedral sheet (7.6:1). Statistically, we are unlikely to observe a significant number of ^{19}F coordinated to two or three Li^+, in adherence with the extended Lowenstein avoidance rule.

NMR Probes of Porous Materials: ^{129}Xe and $^{13}CH_4$

There is a substantial literature describing the use of ^{129}Xe NMR to investigate the pore sizes and site exchange dynamics of mesoporous materials,[1-7] a complete summary of which is beyond the scope of this paper. There is a smaller but growing literature suggesting that $^{13}CH_4$ can probe these properties as well, including results for silicate phases relevant to the clay studied here.[8-11] For instance, for ^{129}Xe in amorphous silicas, Terskikh et al.[5] have shown an excellent correlation between the chemical shift and pore size over a pore size range from ~0.5 to ~ 40 nm. The largest effect on the chemical shift is observed at small pore sizes, and the slope of the relationship decreases at larger pore sizes (their Figure 1). For both $^{13}CH_4$ and ^{129}Xe, rapid exchange between surface-associated sites and the fluid phase greatly affect the observed chemical shift, and Terskikh et al. evaluate their results in terms of a two-site exchange model. There is a generally similar relationship for $^{13}CH_4$, although there are far fewer data and the relationship between pore size and ^{13}C chemical shift is much less well known. For $scCH_4$ with no solids present Ok et al.[18] have recently shown that the resonance is quite narrow (~0.03 ppm FWHH in our data) and becomes progressively less shielded (less negative) by ~ 0.8 ppm with increasing CH_4 pressure from 28.2 to 112.7 bar at T = 307K. They attribute this effect to increasing density of the fluid. For non-porous silica with an average particle diameter of 12 nm, they observe essentially no effect on the chemical shift. For a mesoporous silica with an average pore size of ~4 nm, they observe two resonances. One of these is for the bulk supercritical fluid,

and the other, which is shifted ~ 0.6 ppm to less negative values, represents CH_4 in the mesopores. This change in chemical shift parallels the effect of pore size on the ^{129}Xe chemical shift. The chemical shifts of $^{13}CH_4$ confined in the nano-pores of molecular sieves and methane hydrates (average diameter ~0.5 – 0.6 nm) have even less negative values. For methane hydrates, the chemical shift becomes as much as ~4.2 ppm less negative in the smallest clathrate pores.[10] For molecular sieves, Koskela et al. observe an ~4-5 ppm difference between the bulk gas phase and methane in the nano-pores of $AlPO_4$-11 and SAPO-11.[12-13] These changes, again, parallel those for ^{129}Xe. Thus, both $^{13}CH_4$ and ^{129}Xe are useful probes of porous systems, although the chemical shift range for ^{129}Xe is much larger. Our $^{13}CH_4$ NMR results are interpretable within the context of the literature summarized here.

Supplementary Materials and Methods:

Materials and Sample Preparation

As noted in the main text, the cation exchange procedures used to produce the Ca-, Cs-, and Na-hectorites followed those used previously by our group.[14-16] Samples of purified hectorite are exposed to 1 M solutions of the chloride salt of the desired cation at a solid-to-solution ratio of 500 mg clay/50 mL IEX solution. The clay is suspended in the solution and the suspensions are shaken on a platform rocker for 12-24 hours, after which the clay is isolated by centrifugation and exposed to fresh ion exchange solution. After the second ion exchange, samples are exposed to three rinses in deionized water to remove physically adsorbed cations. Typically, the clay is isolated from the supernatant by centrifuging at ~10,000 g, decanting the supernatant, adding deionized water to the centrifuge tubes, resuspending the clay, and repeating the centrifugation process. Following the final IEX reaction, samples are dried in a vacuum oven at 323 K and -30 mmHg, then ground in an agate pestle and mortar before being sieved to isolate the <150 μm

size fraction. For Pb-hectorite, the as-received sample was exchanged with a saturated $Pb(NO_3)_2$ solution less than 24 hours in age that had been filtered through a 650 nm Millipore filter to remove any suspended nitrate, carbonate, or hydroxide solids before being mixed with the hectorite for ion exchange.

References

1. Jameson, A. K.; Jameson, C. J.; Dedios, A. C.; Oldfield, E.; Gerald, R. E.; Turner, G. L., Xe-129 Magic-Angle-Spinning Spectra of Xenon in Zeolite NaA - Direct Observation of Mixed Clusters of Coadsorbed Species. *Solid State Nucl. Mag.* **1995**, *4*, 1-12.
2. Janicke, M.; Chmelka, B. F.; Larsen, R. G.; Shore, J.; Schmidtrohr, K.; Emsley, L.; Long, H.; Pines, A., 2-Dimensional Xe-129 Exchange NMR Measurements of Xenon Dynamics in Na-A Zeolite. *Stud. Surf. Sci. Catal.* **1994**, *84*, 519-526.
3. Pasquier, V.; Levitz, P.; Delville, A., Xe-129 NMR as a Probe of Gas Diffusion and Relaxation in Disordered Porous Media: An Application to Vycor. *J. Phys. Chem.* **1996**, *100*, 10249-10256.
4. Pasquier, V.; Levitz, P.; Tinet, D.; Delville, A., Xe-129 NMR as a Probe of the Dynamics of Gas Confined in Porous Vycor. *Mag. Reson. Imaging* **1996**, *14*, 971-973.
5. Terskikh, V. V.; Moudrakovski, I. L.; Breeze, S. R.; Lang, S.; Ratcliffe, C. I.; Ripmeester, J. A.; Sayari, A., A General Correlation for the Xe-129 NMR Chemical Shift-Pore Size Relationship in Porous Silica-Based Materials. *Langmuir* **2002**, *18*, 5653-5656.
6. Wernett, P. C.; Larsen, J. W.; Yamada, O.; Yue, H. J., Determination of the Average Micropore Diameter of an Illinois No-6-Coal by Xe-129 NMR. *Energ. Fuel* **1990**, *4*, 412-413.
7. Yang, I. J.; Larsen, R. G.; Shore, J.; Schmidtrohr, K.; Emsley, L.; Long, H.; Pines, A.; Janicke, M.; Chmelka, B. F., 2-Dimensional Magic-Angle-Spinning Xe-129 Exchange NMR-Study of Xenon Energetics and Dynamics in Na-A Zeolite. *Abstr. Pap. Am. Chem. Soc.* **1995**, *209*, 351-CHED.
8. Ok, S.; Hoyt, D. W.; Andersen, A. K.; Sheets, J.; Welch, S. A.; Cole, D. R.; Mueller, K. T.; Washton, N. M., Surface Interactions and Confinement of Methane: A High Pressure Magic Angle Spinning NMR and Computational Chemistry Study. *Langmuir* **2017**, *33*, 1359-1367.
9. Fleyfel, F.; Song, K. Y.; Kook, A.; Martin, R.; Kobayashi, R., Interpretation of C-13 NMR of Methane/Propane Hydrates in the Metastable/Nonequilbirum Region. *J. Phys. Chem.* **1993**, *97*, 6722-6725.
10. Ripmeester, J. A.; Ratcliffe, C. I., Low Temperature Cross Polarization Magic Angle Spinning C-13 NMR of Solid Methane Hydrates: Structure, Cage Occupancy, and Hydration Number. *J. Phys. Chem.* **1988**, *92*, 333-339.
11. Yeon, S.-H.; Seol, J.; Seo, Y.-J.; Park, Y.; Koh, D.-Y.; Park, K.-P.; Huh, D.-G.; Lee, J.; Lee, H., Effect of Interlayer Ions on Methane Hydrate Formation in Clay Sediments. *J. Phys. Chem. B* **2009**, *115*, 1245-1248.
12. Koskela, R.; Ylihautala, M.; Jokisaari, J.; Vaara, J., C-13 NMR of Methane in an AlPO4-11 Molecular Sieve: Exchange Effects and Shielding Anisotropy. *Phys. Rev. B* **1998**, *53*, 14833-14836.

13. Koskela, T.; Ylihautala, M.; Vaara, J.; Jokisaari, J., C-13 NMR of Methane Adsorbed in SAPO-11 Molecular Sieves. *Chem. Phys. Lett.* **1996**, *261*, 425-430.
14. Bowers, G. M.; Singer, J. W.; Bish, D. L.; Kirkpatrick, R. J., Alkali Metal and H_2O Dynamics at the Smectite/Water Interface. *J. Phys. Chem. C* **2011**, *115*, 23395-23407.
15. Bowers, G. M.; Singer, J. W.; Bish, D. L.; Kirkpatrick, R. J., Structural and Dynamical Relationships of Ca^{2+} and H_2O in Smectite/^2H_2O Systems. *Am. Mineral.* **2014**, *99*, 318-331.
16. Bowers, G. M.; Schaef, H. T.; Loring, J. S.; Hoyt, D. W.; Burton, S. D.; Walter, E. D.; Kirkpatrick, R. J., Role of Cations in CO_2 Adsorption, Dynamics, and Hydration in Smectite Clays under in Situ Supercritical CO_2 Conditions. *J. Phys. Chem. C* **2017**, *121*, 577-592.

Supplementary Figures

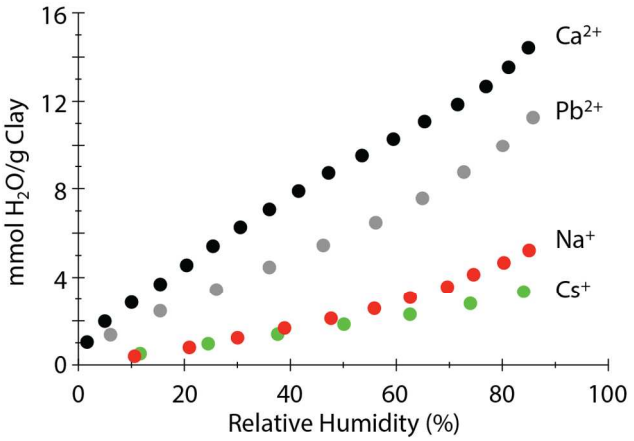

Figure S1. Water uptake by the hectorites with the indicated exchangeable cations as a function of the RH of the $scCH_4$ obtained from the IR titration vapor phase transmission data expressed as mmol H_2O/g clay. The trends are similar to Figure 4 in the main text, but the slopes for the divalent cations are steeper since these data do not account for the H_2O initially present.

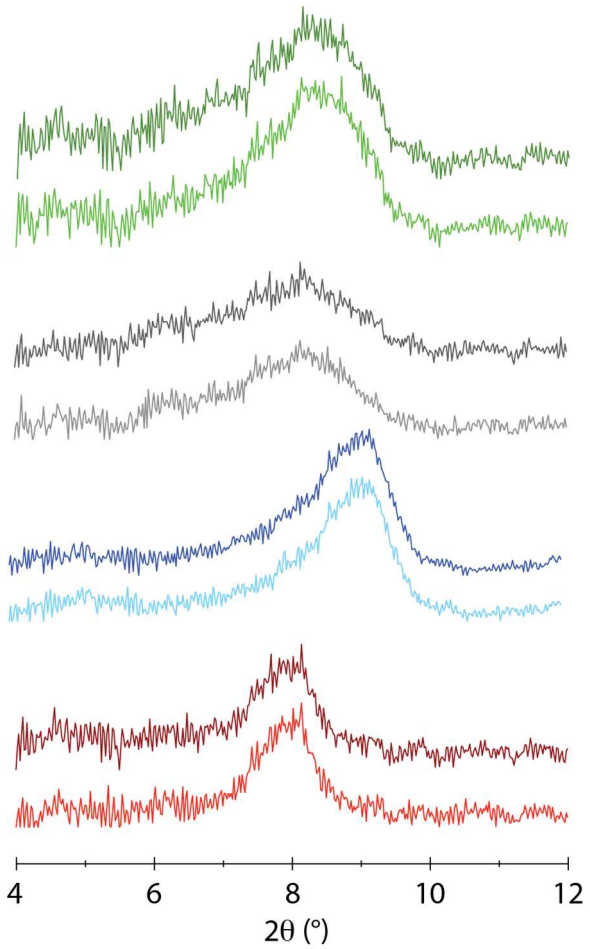

Figure S2. Comparison of the basal reflection region of the four cation exchanged hectorites under vacuum (lower pattern in each set) and in contact with dry CH_4 at 90 bar, 323 K. In all cases, the presence of dry $scCH_4$ under these conditions does not cause observable interlayer expansion, in contrast to the behavior of these samples exposed to dry $scCO_2$.[16] Green = Ca-hectorite, gray = Pb-hectorite, blue = Na-hectorite, and red = Cs-hectorite.

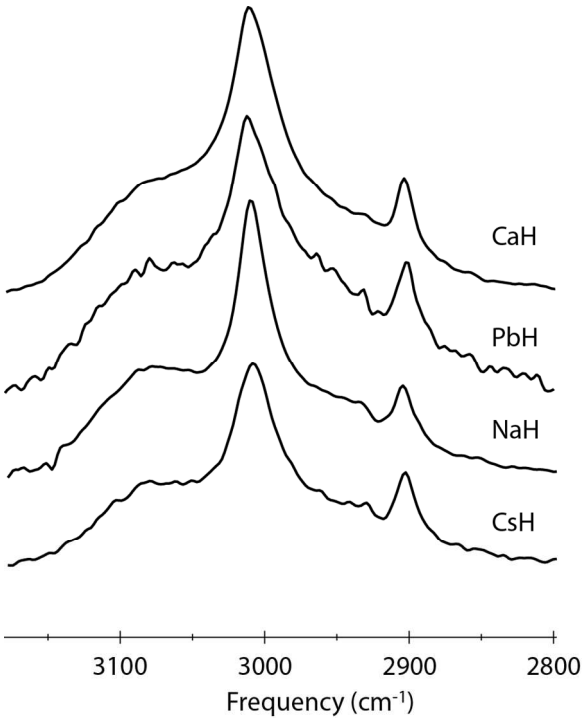

Figure S3. Comparison of the asymmetric C-H stretching region of methane in the i*n situ* ATR-IR spectra of the four cation- exchanged hectorites in contact with dry $scCH_4$. All spectra are normalized with respect to the amount of clay and thus the intensities are directly comparable. Note the symmetry forbidden ν_1 mode for methane at ~2900 cm^{-1}. See the main text for discussion.

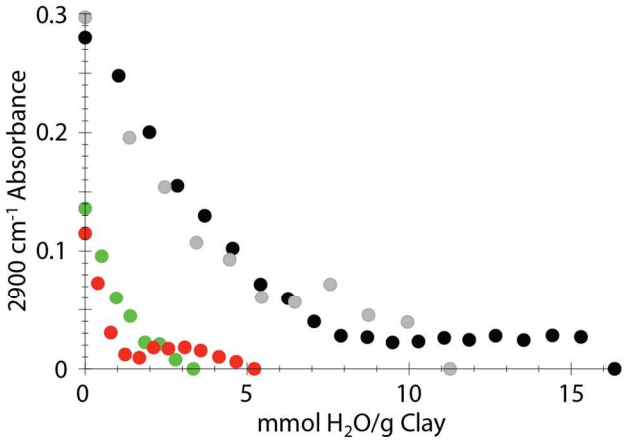

Figure S4. Intensity of the 2900 cm^{-1} ATR-IR band versus the absolute adsorbed H_2O in mmol H_2O/g clay determined from the transmission IR data. The color coding is the same as in Figure S2; red – Na^+, green – Cs^+, grey – Pb^{2+}, black – Ca^{2+}. Note that there is a clear separation between the alkali metal and the divalent cation hectorites within the limits of uncertainty, but that overall, the absorption of the ν_1 band associated decreases in intensity as the H_2O content increases, in agreement with the NMR results for hectorite associated CH_4. The uncertainty on all data points is ±0.0025 absorbance units.

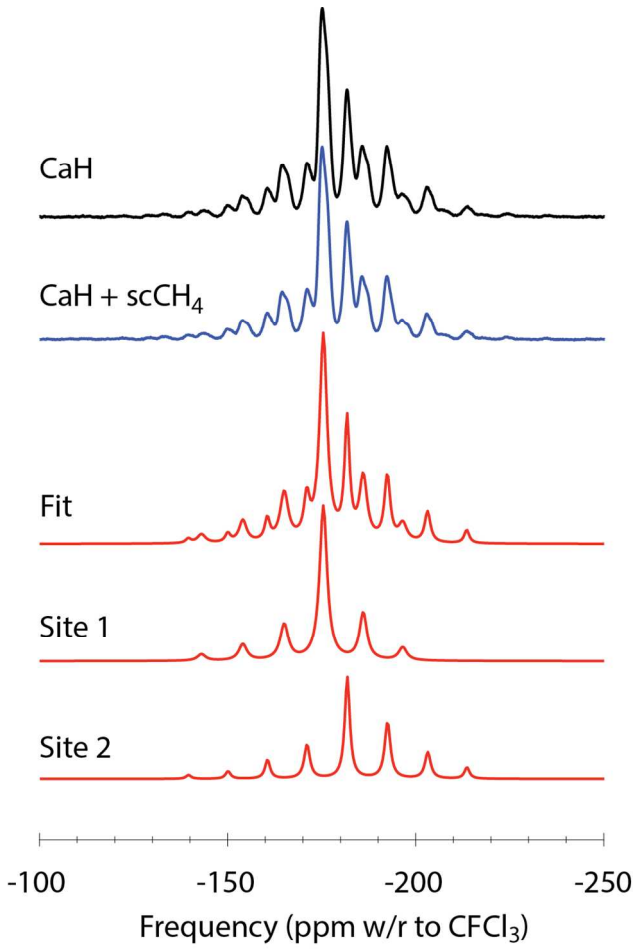

Figure S5. ^{19}F MAS NMR data of vacuum dried Ca-hectorite before and after charging the rotor with $scCH_4$ (90 bar, 323 K). The presence of CH_4 causes essentially no change in the spectra, indicating a lack of direct fluorine-CH_4 interaction at any of the adsorption sites. There are two ^{19}F sites in the clay. We assign the resonance with a smaller chemical shift anisotropy (CSA) pattern (Site 1) to F^- coordinated to three Mg^{2+} in the octahedral layer and the resonance with the larger CSA pattern (Site 2) to F^- coordinated to two Mg^{2+} and one Li^+ in the octahedral layer.

Supplementary Tables

Table S1. Masses and moles of each clay sample in the NMR experiments.

		Masses (g)				Moles		
Sample	Humidity	Clay	H_2O beyond vacuum state	CH_4	ΔCH_4	Clay	H_2O beyond vacuum state	CH_4
CH_4				0.0082				0.000511
CaH	vac	0.1431	0	0.0066	-0.0002	0.000374	0	0.000411
CaH	43%	0.1431	0.0095	0.0054	-0.0044	0.000374	0.000527	0.000337
CaH	100%	0.1306	0.0335	0.0039	0.0002	0.000341	0.001859	0.000243
PbH 2017	vac	0.1636	0.002	0.0065	-0.0003	0.000436		0.000405
PbH 2017	43%	0.1636	0.0105	0.0045	0.0003	0.000436	0.000583	0.000281
PbH 2017	100%	0.1636	0.0175	0.0035	Crashed	0.000432	0.000971	0.000218
CsH 2015	vac	0.1349	0	0.0067	-0.0048	0.000320	0	0.000418
CsH 2015	43%	0.1349	0.0046	0.0062	0.0004	0.000320	0.000255	0.000386
CsH 2015	100%	0.1349	0.0117	0.0050	N/A	0.000320	0.000649	0.000312
NaH 2015	vac	0.1576	0	0.0053	-0.0004	0.000411	0	0.000330
NaH 2015	29%	0.1577	0.0027	0.0041	-0.0006	0.000411	0.000150	0.000256
NaH 2015	43%	0.1576	0.0043	0.0043	1E-04	0.000411	0.000239	0.000268
NaH 2015	100%	0.1597	0.0083	0.0040	0.0009	0.000411	0.000461	0.000249
NaH 2009	vac	0.1361	0	0.0066	0.0004	0.000355	0	0.000411
NaH 2009	43%	0.1361	0.0045	0.0056	-0.0004	0.000355	0.000248	0.000350
NaH 2009*	100%	0.1361	0.0178	0.0047	-0.0001	0.000355	0.000990	0.000294

*This sample was equilibrated at RH for 44 hours compared to 12-24 hours for all other samples.

Table S2. Mole ratios of species in the NMR experiments. Note that we are unable to quantify the amount of water present in the vacuum dried samples, and use them as a reference point (thus their assignment to 0 in the third and fourth columns). The values in the final column have an uncertainty of ~10%.

Sample	Humidity	$X_{water/cation}$	$X_{water/CH4}$	$X_{CH4/cation}$	$X_{interlayerCH4/cation}$
CH_4					
CaH	vac	0	0	6.3	1.50
CaH	43%	8.1	1.6	5.1	1.48
CaH	100%	31.1	7.6	4.1	-
PbH 2017	vac	0	0	5.3	1.82
PbH 2017	43%	7.6	2.1	3.7	0.78
PbH 2017	100%	12.9	4.5	2.9	-
CsH 2015	vac	0	0	3.7	0.39
CsH 2015	43%	2.3	0.66	3.5	0.35
CsH 2015	100%	5.8	2.1	2.8	-
NaH 2015	vac	0	0	2.3	0.48
NaH 2015	29%	1.0	0.59	1.8	-
NaH 2015	43%	1.7	0.89	1.9	-
NaH 2015	100%	3.2	1.9	1.7	-
NaH 2009	vac	0	0	3.3	-
NaH 2009	43%	2.0	0.71	2.8	-
NaH 2009*	100%	8.0	3.4	2.4	-

*This sample was equilibrated at RH for 44 hours compared to 12-24 hours for all other samples.